ELECTROCHEMICAL IMPREGNATION OF NICKEL HYDROXIDE IN POROUS ELECTRODES

Kuo-Chuan Ho and Jacob Jorné
The University of Rochester
Rochester, New York 14627

The electrochemical impregnation of nickel hydroxide in porous electrode has been investigated both experimentally and theoretically. The loading level and plaque expansion were the most important parameters to be considered. The effects of applied current density, stirring, ratio of solution to electrode volume and pH have been identified. A novel flow-through electrochemical impregnation is proposed in which the electrolyte is forced through the porous nickel plaque. The thickening of the plaque can be reduced while maintaining high loading capacity. A mathematical model is presented which describes the transport of the nitrate, nickel and hydroxyl ions and the consecutive heterogeneous electrochemical reduction of nitrate and the homogeneous precipitation reaction of nickel hydroxide. The distributions of precipitation rate and active material within the porous electrode are obtained. A semi-empirical model is also proposed which takes into account the plugging of the pores.

INTRODUCTION

Early in the research and development of nickel hydroxide electrodes, effort was focused on achieving high loading of active material into sintered plaques in order to increase the specific energy of battery systems. Higher specific energies were obtained by increasing the sinter porosity, varying the powder type, addition of lightweight inert filler material, and increasing the impregnation rate by raising the solution temperature up to its boiling point. However, higher porosity results in a structurally weak material which cannot endure the stresses involved in impregnation and cycling. In addition, Seiger et. al. [1] have shown that as the plaque becomes more porous, the tendency to blister and shed increases which leads to a decrease in utilization efficiency, i.e., the amount of active material that is electrochemically available during discharge (the measured capacity) divided by the amount of active material impregnated into the porous sintered plaque (the theoretical capacity). They experimentally found that the utilization efficiency linearly depends upon sinter porosity over a wide range of practical porosities used. Ford and Baer [2] have also shown that utilization efficiency begins to decrease markedly at a loading of 2.1 g/cm^3.

In recent years the trend has been to somewhat sacrifice loading in order to achieve longer design life. Lim [3] found that increasing the loading level of the nickel electrode could result in a better initial performance, which is not necessarily an indication of good life performance. This is because several physical changes occur inside the porous structures during cycling, especially at high loading, and adversely shorten the cycle life. These structural changes can be related to the dimensional expansion of the electrode. One may therefore infer that there must exist an optimum loading level for a long nickel electrode cycle life. Indeed, Lim [3]

PRECEDING PAGE BLANK NOT FILMED

has shown that the loading level of the active material affects the cycle life of the nickel electrodes, and reported an optimum loading of 1.6 g/cm^3 using the sintered nickel plaque of 82 % porosity and 29 $mils$ thickness. At this loading level, only about 40 % of the void volume is actually filled with active material.

With conventional chemical impregnation, it is difficult to deposit the active material inside the pores of the plaque without precipitation in the bulk solution and on the outside of the plaque surface. Studies on cathodic electrochemical impregnation have probably been an impetus of the trend to reduce loading level, since electrodes fabricated by electrochemical impregnation exhibit improved utilization with reduced loading. Nevertheless, with cathodic electrochemical impregnation, it is well known that thickening of plaques usually occurs even after the electrode was freshly manufactured [1, 4, 5, 6]. This is especially true at high impregnation current densities. It has been shown that to some extent agitation does retard the formation of nickel hydroxide on the surface. It may therefore be expected that an electrode impregnated under flow–through conditions would suppress surface loading by sacrificing process efficency. In this study, cathodic electrochemical impregnation has been conducted under various flow configurations. The effect of flow rate on loading level and thickening of nickel electrodes has also been studied.

EXPERIMENTAL

One of the motivating factors in the present approach was to identify the effect of flow on the loading and thickening of nickel electrodes. These topics are important in designing and processing plaques into positive electrodes with higher energy densities and longer cycle life.

Porous sintered nickel plaques supplied by General Electric were used in the flow–through electrochemical impregnation studies. The wettability of the plaques was also tested. Both tube and rectangular–type modified cells were used for the experiments. The only design change has been the connection of the external conduits to the cell ends so that the electrolyte can flow through the cathode. A reservoir containing 100 ml of 3.0M $Ni(NO_3)_2$ solution was used in order to provide sufficient electrolyte and regulate the flow. In the tube–type cell, the nickel plaque was screwed in, clamped and tightly sealed with 0–rings between two glass tubes. This procedure frequently caused cracking and damage to the plaque. Later, this problem was solved by using a rectangular–type cell. Another advantage of the rectangular–type cell over the tube–type cell is that the former can operate at a very low flow rate (0.06 $cm^3/cm^2 \cdot min$), using gravity feeding. The tube–type and the rectangular–type cells with the counterelectrode placed in a downstream position are shown in Figures 1 and 2, respectively. By reversing the flow direction, both tube–type and rectangular–type cells can operate with upstream counterelectrode placement. Electrodes were visually inspected after impregnation. Electrode thickness and weight gain were measured in order to characterize the electrodes. The electrode separations in the tube–type and rectangular–type cells were 8.5 cm and 4.0 cm, respectively. Initially, the pH of solution was adjusted to 3.0 or 4.5, depending on the purpose of each run.

Auxiliary experiments have been carried out in a thicker electrode which consists of two nickel electrodes with a counterelectrode placed in the upstream position. The second electrode is made electrochemically inert by winding Teflon tape

around the edges, thus, any $Ni(OH)_2$ particles escaping from the first electrode were collected subsequently by the second electrode, which acts as a filter.

In order to have better utilization of the porous electrode, two–side impregnation was performed under stagnant and flow–through conditions. Figure 3 shows the electrodes and flow configurations. Figure 3(a) represents a stagnant, two–side impregnation where each side was separately impregnated for equal period of time. Figure 3(b) represents a flow–through electrode in an upstream counterelectrode configuration with gravity fed electrolyte. Once again, the impregnation time of each side was the same and the current and flow were always in the same direction.

Finally, experiments were also conducted for two–side impregnation where both sides were impregnated simultaneously. Figure 4 shows the electrode and flow configurations for simultaneous two–side impregnation. Figure 4(a) represents a stagnant, two–side impregnation, while Figure 4(b) represents a flow–through two–side impregnation where the flow was periodically reversed. Thus, each side was alternately exposed to an upstream and downstream positioning of the counter electrode.

RESULTS AND DISCUSSION

Figure 5 compares the loading level under stagnant and flow conditions in a tube–type cell with the counterelectrode placed in the downstream position. In both cases, limiting loading levels were approached, however, lower loading was obtained under flow through conditions ($V_x = 0.30\ cm/min$). Figure 6 shows a similar plot for a stagnant and flow–through impregnation carried out in a rectangular–type cell. Two velocities ($V_x = 0.06\ cm/min$ and $0.30\ cm/min$) were studied and the loading data suggest that the higher the flow velocity, the lower the loading level. The loading curve under flow conditions is characterized by two plateaus. The first plateau is obtained under flow–through conditions, while the second one appears to be reached after the electrode is plugged and can be regarded as a stagnant electrode. The transition region defines the onset time for electrode plugging. The electrode was plugged after 75 min operation, as can be seen from Figure 6. This was observed experimentally when the electrolyte overflowed from one compartment to the other. Figure 7 presents the plaque expansion vs. loading level for the three loading curves shown in Figure 6. The experimental results show that a very small flow rate ($V_x = 0.06\ cm/min$) can retard the formation of nickel hydroxide on the surface. Under carefully controlled flow conditions, one might expect to obtain a uniformly distributed $Ni(OH)_2$ precipitation without surface deposit. However, under flow–through conditions the loading level is substantially lower, due to the removal of the newly–formed $Ni(OH)_2$ by convection. Therefore, it is expected that an optimal flow–through velocity exists such that a longer cycle life is achieved by sacrificing loading and by eliminating surface precipitation. It is also expected that the distribution of $Ni(OH)_2$ is more uniform in a flow–through configuration.

Figure 8 presents loading curves for stagnant and flow–through impregnation conducted in a rectangular–type cell with the counterelectrode placed in the upstream position. The shape of the curves is similar to those shown in Figure 6 for a downstream positioning of the counterelectrode. Once again, the overflow of electrolyte was observed. However, in a flow–through operation, an upstream place-

ment of the counterelectrode reached stagnant behavior faster than a downstream placement, 45 min for upstream placement as compared to 75 min for downstream placement. This is because of the nonuniformity of precipitation and an earlier plugging of the pores. The corresponding plot for plaque expansion vs. loading level is shown in Figure 9. A visual examination of the electrodes after impregnation shows that when the electrolyte flows in the same direction as the current (upstream counterelectrode), a more uniform distribution of active material inside the plaque is obtained as compared to a downstream placement of the counterelectrode in which the electrolyte and current flow in opposite directions. When the counterelectrode is placed in the upstream position, the ohmic potential drop favors precipitation at the front while mass transfer of hydroxyl ions favors precipitation at the back resulting in fairly uniform distribution of active material.

Figure 10 shows the same loading experiment to that in Figure 8 except under a lower initial pH value ($pH_o = 3.0$ vs. 4.5). The experimental data show that the pH_o has little or no effect on the loading level. A plot of plaque expansion vs. loading level with $pH_o = 3.0$, as shown in Figure 11, exhibits a very similar trend as that of $pH_o = 4.5$. This is because the internal pH (inside the pores) does not vary with the external pH (in the bulk), and it is the pH value inside the pores which determines the loading characteristics of the process.

Experimentally, it is interesting to notice that there was always a loss of active material when impregnation was carried out in the flow–through conditions, regardless of the electrode placement. The loss of $Ni(OH)_2$ reaches as high as 50 % compared to the stagnant case, especially before the pores were plugged. The colloidal form of $Ni(OH)_2$ was carried away and precipitated at the bottom of the cell and in the reservoir. Later, the lost active material was collected by an additional porous nickel electrode with insulated edges attached to the working electrode. The flow rate was 0.06 $cm^3/cm^2.min$, and the counterelectrode was placed in the upstream position. It was observed that some of the escaping $Ni(OH)_2$, in powder form of light green color, was presented in the gap between the two electrodes. Agglomerations of this powder, which apparently had escaped from the first electrode, was found randomly distributed over the surface of the second electrode. Weight gain analysis of the first electrode was consistent with the loading data obtained in Figure 8 under the same flow condition. However, the weight gain of the second inert electrode revealed that a significant amount of $Ni(OH)_2$ was hydrodynamically washed out. The weight gain of the two electrodes under flow–through conditions is shown in Figure 12 and compared with the data for stagnant and flow–through operations with a single electrode. The loading with double electrodes under flow–through conditions is higher for the stagnant electrode, apparently because of the continuous supply of $Ni(NO_3)_2$ to the porous electrode in the flow–through case.

Figures 13 and 14 show the loading level and plaque expansion with two–side impregnation for stagnant and flow–through conditions. The data indicated by the blank triangles represents two–side impregnation with time equally divided for each side, while the data with black triangles represent two–side impregnation, where each side receives cathodic impregnation periodically for 2.5 min. The trends are similar to the earlier results with one–side impregnation. The electrode becomes plugged after a 45 min operation. However, a comparision of Figure 9 with Figure 14 reveals that, regardless of flow conditions, a better electrode can be obtained with two–side impregnation in terms of plaque thickening. At the same loading

level, plaque expansion is reduced by nearly 50 % in two–side impregnation both for stagnant and flow–through conditions. This is because a better utilization of the electrode is achieved in two–side impregnation.

The loading level and plaque expansion for simultaneous two–side impregnation are shown in Figures 15 and 16, respectively. It can be seen that, with a combination of upstream and downstream counterelectrode and a small flow rate $(V_x = 0.06 \ cm/min)$ can reduce surface loading without significantly sacrificing process efficiency, as shown in Figure 15. However, a close examination after electrochemical impregnation reveals that a moderate plaque thickening does exist even with flow–through operation. This is because stagnant behavior is reached in a very short time (less than 15 min) as a result of pore–plugging and, therefore, further loading of the surface is preferred.

MATHEMATICAL MODEL

Electrochemical impregnation is by nature an unsteady state process owing to structure variation as the process proceeds. The complexity of the problem involving structural change as well as escape of $Ni(OH)_2$ has made a quantitative description difficult. However, pseudo–steady state is a good assumption for porous electrodes under flow–through conditions [7, 8]. In this section, a model of flow–through porous electrode suitable for electrochemical impregnation is presented and the distributions of active material and loading capacity are derived. Finally, a critical, pore plugging time, is analytically calculated at which the porosity at the front of electrode reaches half of its initial value [9]. The predicted plugging time is compared with experimental data. This pore–plugging process is very similar to the one mentioned in the recovery of copper ions [9].

Figure 17 represents flow–through electrochemical impregnation with the counterelectrode placed downstream. $x = 0$ represents the flow inlet and $x = L$ represents the outlet. No precipitation occurs within region I $(0 \leq x \leq \delta_o)$, where δ_o is the position of the onset of the precipitation reaction. Precipitation occurs within region II.

The following equations for region I and II can be written as:

$$\frac{\partial(\epsilon C_1)}{\partial t} = \epsilon D_1 \frac{\partial^2 C_1}{\partial x^2} - V_x \frac{\partial C_1}{\partial x} + \epsilon D_1 \frac{\partial}{\partial x}(C_1 \frac{\partial \xi}{\partial x}) - Aj_{1n} \qquad (1)$$

$$\frac{\partial(\epsilon C_2)}{\partial t} = \epsilon D_2 \frac{\partial^2 C_2}{\partial x^2} - V_x \frac{\partial C_2}{\partial x} - 2\epsilon D_2 \frac{\partial}{\partial x}(C_2 \frac{\partial \xi}{\partial x}) - R_{ppt} U(x - \delta_o) \qquad (2)$$

$$\frac{\partial(\epsilon C_3)}{\partial t} = \epsilon D_3 \frac{\partial^2 C_3}{\partial x^2} - V_x \frac{\partial C_3}{\partial x} + \epsilon D_3 \frac{\partial}{\partial x}(C_3 \frac{\partial \xi}{\partial x}) - 2R_{ppt} U(x - \delta_o) + 9Aj_{1n} \qquad (3)$$

$$-C_1 + 2C_2 - C_3 = 0 \qquad (4)$$

$$j_{1n} = \frac{S_1}{nF} i_o[e^{(1-\beta)n\xi} - e^{-\beta n\xi}] \qquad (5)$$

$$[\kappa^{-1} + \sigma^{-1}]^{-1} \frac{\partial^2 \xi}{\partial x^2} = \frac{nF^2}{S_1 RT} Aj_{1n} \qquad (6)$$

In addition, the following equations are also valid in the precipitation region II:

$$C_2 C_3^2 = K_{sp} \tag{7}$$

$$\frac{\partial \epsilon}{\partial t} = -M_j \rho_j^{-1} R_{ppt} \tag{8}$$

where subscripts 1, 2 and 3 corresponding to NO_3^-, Ni^{+2} and OH^-, respectively. $U(x - \delta_o)$ is the unit step function. Eqs. (1), (2) and (3) represent the mass balance equations for NO_3^-, Ni^{+2} and OH^-, respectively. Eq. (4) is the electroneutrality condition. Eq. (5) expresses the flux of reacting nitrate in terms of the Butler–Volmer equation. Eq. (6) is the potential equation inside the porous electrode. Eq. (7) is the fast equilibrium condition between Ni^{+2} and OH^-. Eq. (8) is the mass balance equation for $Ni(OH)_2$. For the case of pseudo–steady state operation, $C_i \frac{\partial \epsilon}{\partial t} \gg \epsilon \frac{\partial C_i}{\partial t}$, or $C_i(x,t) \simeq C_i(x)$ $(i = 1,2,3)$. Combining Eq. (8) with the assumption that $C_j \gg C_i$ $(i = 1,2,3)$, Eqs. (1), (2) and (3) become

$$\epsilon D_1 \frac{d^2 C_1}{dx^2} - V_x \frac{dC_1}{dx} + \epsilon D_1 \frac{d}{dx}\left(C_1 \frac{\partial \xi}{\partial x}\right) - A j_{1n} = 0 \tag{9}$$

$$\epsilon D_2 \frac{d^2 C_2}{dx^2} - V_x \frac{dC_2}{dx} - 2\epsilon D_2 \frac{\partial}{\partial x}\left(C_2 \frac{\partial \xi}{\partial x}\right) - R_{ppt} U(x - \delta_o) = 0 \tag{10}$$

$$\epsilon D_3 \frac{d^2 C_3}{dx^2} - V_x \frac{dC_3}{dx} + \epsilon D_3 \frac{\partial}{\partial x}\left(C_3 \frac{\partial \xi}{\partial x}\right) - 2 R_{ppt} U(x - \delta_o) + 9 A j_{1n} = 0 \tag{11}$$

The dimensionless overpotential distribution can be obtained under the case of low irreversibility, therefore, the concentration profile of nitrate can be calculated. The concentration distributions of nickel and hydroxyl ions in region II can be obtained by eliminating the rate of precipitation and using the equilibrium condition, Eq. (7). The following section shows the analysis of flow–through electrochemical impregnation during early stages of operation.

ANALYSIS

Analytical solution can only be obtained with the assumptions that linear kinetics and constant specific surface area and porosity are obeyed. It can be shown that the approximate concentration profiles for this systems are [10]

$$C_1^{I \& II} \simeq C_{1o} - p_1 a_1^{-1} \sinh(mx) \tag{12}$$

$$C_2^I \simeq C_2|_{\delta_o} \simeq C_{2o} \tag{13}$$

$$C_2^{II} \simeq C_2|_{\delta_o} - (9/2) p_1 a_1^{-1} m(x - \delta_o) \tag{14}$$

$$C_3^I \simeq C_{3o} - p_3 a_3^{-1} \sinh(mx) \tag{15}$$

$$C_3^{II} \simeq K_{sp}^{1/2}[C_2|_{\delta_o} - (9/2) p_1 a_1^{-1} m(x - \delta_o)]^{-1/2} \tag{16}$$

where $a_1 = V_x/\epsilon D_1$, $a_3 = V_x/\epsilon D_3$, $p_1 = iS_1/nF\epsilon D_1 sinh(mL)$, $p_3 = -9iS_1/nF\epsilon D_3 sinh(mL)$. For typical impregnation conditions in an acidic solution $(pH = 3-6)$, $C_{3o} = 10^{-14}-10^{-11}$ $mole/cm^3$, $C_{2o} = 3\times10^{-3} mole/cm^3$, $T = 90°C$, however, $C_3|_{\delta_o} \simeq (K_{sp}C_{2o}^{-1})^{1/2} = 1.24 \times 10^{-9}$ $mole/cm^3$, therefore, $C_{3o} \ll C_3|_{\delta_o}$. According to Eq. (15)

$$C_3|_{\delta_o} = -p_3 a_3^{-1} \sinh(m\delta_o) \simeq -p_3 a_3^{-1} m\delta_o = \frac{9iS_1 m\delta_o}{nFV_x \sinh(mL)} \qquad (17)$$

in the case when $mL \leq 0.5$, $\sinh(mL) \simeq mL$, Eq. (17) gives

$$(\frac{\delta_o}{L}) = \frac{nFV_x C_3|_{\delta_o}}{9iS_1} \qquad (18)$$

assuming that $i = -100$ mA/cm^2, $V_x = 0.06$ cm/min, $C_3|_{\delta_o} = 2.1 \times 10^{-9}$ $mole/cm^3$, the calculated value of (δ_o/L) is on the order of 10^{-6}, which practically means that the pH of the solution inside the pores is always high enough to cause precipitation within the whole electrode. It is clear that for a constant inlet concentration of nickel ions $(C_{2o} = const.)$, the higher the flow velocity, the higher the value of δ_o. On the other hand, for a constant flow velocity and constant inlet concentration of nickel ion, the higher the applied current density, the lower the value of δ_o. At constant current density and flow velocity, increasing C_{2o} will decrease $C_3|_{\delta_o}$ and, hence, decrease δ_o. The expressions for rate of precipitation, distribution of nickel hydroxide, porosity and loading are presented below.

· **Rate of Precipitation:**

The rate of precipitation can be obtained from Eqs. (10) and (14) by neglecting diffusion and migration

$$R_{ppt} = -V_x \frac{dC_2}{dx} = -V_x[-(9/2)p_1 a_1^{-1} m] \qquad (19)$$

or

$$R_{ppt} = (1/2)V_x C_3|_{\delta_o} \delta_o^{-1} = (9/2)(\frac{iS_1}{nFL}) \qquad (20)$$

In fact, Eq. (20) expresses the rate of precipitation in the limit when $t \to 0$, i.e., $R_{ppt}(x, t = 0)$. By differentiating Eq. (10) with respect to time and using Eq. (8), one obtains

$$R_{ppt}(x,t) = R_{ppt}(x,t = 0)e^{-g(x)t} \qquad (21)$$

where

$$g^{-1}(x) \equiv \frac{C_j}{[D_2 \frac{d^2 C_2}{dx^2} - 2D_2 \frac{d}{dx}(C_2 \frac{d\xi}{dx})]} \qquad (22)$$

$g^{-1}(x)$ is the local characteristic time of the system if diffusion and migration are the mechanisms for the transport process. After substituting the expressions for C_2 and ξ, one gets

$$g(x) = C_j^{-1}(-2D_2/L^2)(FiL/\kappa RT)(C_{2o} - 9p_1 a_1^{-1} mx) \qquad (23)$$

Typical operating conditions and physical parameters are: $C_{2o} = 3 \times 10^{-3}$ $mole$ $/cm^3$, $i = -100$ mA/cm^2, $T = 90°C$, $D_2 = 0.72 \times 10^{-5}$ cm^2/s, $\kappa = 0.4$ mho/cm, $L = 0.1$ cm, $C_j = 4.15/92.72$ $mole/cm^3$. Therefore, 10^6 $sec \leq g^{-1}(x) \leq 10^7$ sec. This confirms the fact that for porous electrodes operating under flow–through conditions, the convective term is dominant. Thus, the real impregnation time is much shorter than the characteristic time

$$t/g^{-1}(x) \ll 1 \tag{24}$$

An examination of the expression for the rate of precipitation under flow–through conditions (Eq. (21)) reveals the existence of a time–invariant reaction rate

$$R_{ppt}(x,t) = R_{ppt}(x, t = 0) \tag{25}$$

However, according to Eq. (20), the initial rate of precipitation is space–invariant. Finally, one concludes that under flow–through conditions, the rate of precipitation is time and space–invariant, as compared to the relatively nonuniform rate for static operation. With knowledge of the rate of precipitation, one can calculate the distribution of nickel hydroxide, the loading level and the porosity distribution.

· **Distribution of Nickel Hydroxide:**

The concentration of precipitated nickel hydroxide is given by

$$C_{ppt}(x,t) = \int_o^t R_{ppt}(x,t)dt = (1/2)V_x C_3|_{\delta_o}\delta_o^{-1}\frac{1}{g(x)}[1 - e^{-g(x)t}] \tag{26}$$

In the case when $g(x) \to 0$, Eq. (26) takes the form

$$C_{ppt} = R_{ppt}t = (1/2)V_x C_3|_{\delta_o}\delta_o^{-1}t = (9/2)(iS_1/nFL)t \tag{27}$$

· **Loading Level:**

The local loading is given by integrating the rate of precipitation over time

$$W_g(x,t) = \int_o^t R_{ppt}(x,t)M_j\epsilon_o^{-1}dt = M_j\epsilon_o^{-1}C_{ppt}(x,t) \tag{28}$$

and the average loading is given by

$$\bar{W}_g(t) = M_j\epsilon_o^{-1}R_{ppt}t \tag{29}$$

The rate of precipitation is obtained from Eq. (20). Therefore, Eq. (29) becomes

$$\bar{W}_g(t) = -M_j(\epsilon_o L)^{-1}(9i/16F)t = S_F t \tag{30}$$

where

$$S_F = -M_j(\epsilon_o L)^{-1}(9i/16F) \tag{31}$$

Equation (30) relates the theoretical loading capacity to the applied current density by Faraday's law during the early stages of the process, regardless of flow conditions. However, with a flow–through single electrode, the real loading rate is only about 50 % of its theoretical value even in the early stages. The loss in capacity is believed to be caused by hydrodynamic flow which carries away some of the $Ni(OH)_2$. The recovery of Faraday's behavior by using a flow through double electrode with the second electrode serving as a filter and the agreement with Faraday's slope confirm this finding (Figure 12).

The loading characteristics of a flow–through double electrodes can be represented by a semi–empirical equation where the rate of precipitation is proportional to the fraction of maximum loading which is available for further precipitation

$$\frac{d\bar{W}_g(t)}{dt} = S_F(1 - \bar{W}_g/\bar{W}_{g,max}) \tag{32}$$

By integraion one obtains

$$\bar{W}_g(t) = \bar{W}_{g,max}\left(1 - e^{-S_F t/\bar{W}_{g,max}}\right) \tag{33}$$

where $\bar{W}_{g,max}$ is the maximum loading capacity under flow–through conditions, and can be estimated from the density of nickel hydroxide, ρ_j, i.e.,

$$\bar{W}_{g,max} = \rho_j \tag{34}$$

· **Porosity Distribution:**

By integrating Eq. (8), one may obtain the porosity distribution

$$\epsilon(x,t) = \epsilon_o - C_j^{-1} R_{ppt}(x,t=0)[\frac{1}{g(x)}(1 - e^{-g(x)t})] \tag{35}$$

In the limit when $g(x) \to 0$, Eq. (25) becomes

$$\epsilon(x,t) = \epsilon_o - C_j^{-1} R_{ppt}(x,t=0)t \tag{36}$$

A critical pore plugging time (t_p), can be defined for which $\epsilon(x = L, t_p) = \epsilon_o/2$

$$t_p = \frac{\rho_j \epsilon_o}{2M_j R_{ppt}(x = L, t = 0)} \tag{37}$$

where $R_{ppt}(x = L, t = 0)$ represents the initial rate of precipitation at the front of the electrode and is also equal to the rate at pseudo–steady state because the rate of precipitation is time and space invariant. Equation (29) indicates that from the

293

slope of the loading curve, one may calculate the real rate of precipitation, which is an important and practical quantity under flow–through operation. Hence

$$R_{ppt}(x,t) = R_{ppt} = M_j^{-1} \epsilon_o S_f \qquad (38)$$

where S_f represents the initial slope of the loading curve under flow– through conditions. Substitution of Eq. (38) into Eq. (37) gives

$$t_p = \rho_j / 2S_f \qquad (39)$$

The loading curve in Figures 6 and 8 gives S_f a value of 2×10^{-2} $g/cm^3.min$ and 2.7×10^{-2} $g/cm^3.min$ for downstream and upstream counterelectrode placement, respectively. The predicted pore plugging time for downstream and upstream counterelectrode placement are 100 min and 75 min, respectively. This is in reasonable agreement with the experimental onset time of plugging, which can be identified from Figures 6 and 8 as 75 min and 45 min for downstream and upstream counterelectrode placement, respectively. Furthermore, escape of nickel hydroxide carried away by the flow may result in earlier plugging.

CONCLUSIONS AND SUMMARY

It has been experimentally shown that the thickening of plaques during electrochemical impregnation of nickel hydroxide electrodes can be reduced by using a flow–through porous cathode. The effects of flow rate, flow direction, initial pH as well as electrode configuration on loading level and plaque expansion have been identified.

In the case of an electrode impregnated on one side, flow–through of electrolyte reduces the formation of surface deposit, but at the same time it also reduces the loading level. The cause of the decrease in loading has been identified to be the escape of $Ni(OH)_2$, as the newly formed active material was continuously exposed to flow. A flow rate on the order of 0.06 $cm^3/cm^2.min$ may cause such a loss. Visually, a cell configuration in which the electrolyte flows in the same direction as the current (upstream counterelectrode) gives uniform distribution of $Ni(OH)_2$ and reduces the plaque thickening. A cell configuration in which the porous nickel plaque is sandwiched between two anodes with an upstream position for the active anode gives the best electrode characteristics.

A pseudo–steady state model suitable for electrochemical impregnation under flow–through condition has been developed and analyzed. The analysis allows us to predict theoretically the onset time for plugging. The predicted pore plugging time is in reasonable agreement with the experimental results.

The experimental results provide an insight to the loading capacity and thickening of electrode during electrochemical impregnation under stagnant and flow–through conditions. It is suggested that by a careful selection of the flow rate, flow direction and electrode configuration, optimum conditions for the fabrication of nickel hydroxide electrodes can be achieved.

REFERENCES

[1] H. N. Seiger, V. J. Puglisi, P. F. Ritterman, and D. F. Pickett, "High Energy Density Sintered Plate Type Sealed Nickel Cadmium Battery Cells. Part I. The Positive Electrode/Plaque Relationships,"Proceedings of the 9th IECEC, 868, San Francisco, CA (1974).

[2] F. E. Ford and D. A. Baer, "Design and Manufacturing Changes Incorporated in the Nickel–Cadmium Space Cell during the Past Decade, "Proceedings of the Symposium of Battery Design and Optimization, vol. 79-1, pp.114–127, The Electrochemical Society, Pennington, NJ (1979).

[3] H. S. Lim, "Long Life Nickel Electrodes for Nickel–Hydrogen Cells, "NASA CR–174815 (1984).

[4] V. J. Puglisi, H. N. Seiger, and D. F. Pickett, "High Energy Density Sintered Plate Type Nickel–Cadmium Battery Cells. Part II. Electrochemical Impregnation Methods to Produce Nickel Oxide Electrodes, "Proceedings of the 9th IECEC, 873, San Francisco, CA (1974).

[5] P. K. Ng and E. W. Schneider, "Distribution of Nickel Hydroxide in Sintered Nickel Plaque Measured by Radiotracer Method during Electroimpregnation, "J. Electrochem. Soc., 133, 17 (1986).

[6] H. N. Seiger, Comments, J. Electrochem. Soc., 133, 1524 (1986).

[7] R. C. Alkire, E. A. Grens II, and C. W. Tobias, "A Theory for Porous Electrodes Undergoing Structural Change by Anodic Dissolution, "J. Electrochem. Soc., 116, 1328 (1969).

[8] K. C. Ho and J. Jorné, "A Pseudo–Steady State Theory for Flow–Through Porous Electrodes Undergoing Structural Change, "Ext. Abs. # 63, The Electrochem. Soc., Meeting, Las Vegas, Nevada (1985).

[9] D. N. Bennion and J. Newman, "Electrochemical Removal of Copper Ions from Very Dilute Solutions, "J. Appl. Electrochem., 2, 113 (1972).

[10] K. C. Ho, "Electrochemical Impregnation of Nickel Hydroxide in Porous Electrodes, "Ph. D. Dissertation, The University of Rochester, NY (1987).
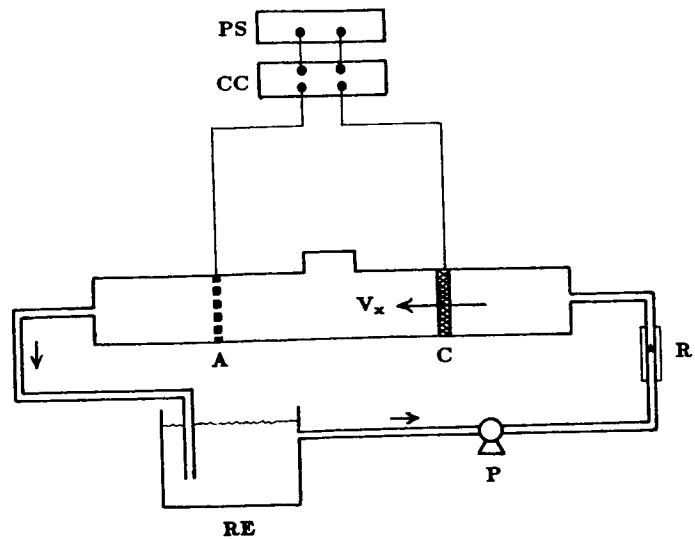
Figure 1. The Flow Tube–Type Cell with Anode Placed in Down-
         stream (A: Anode, C: Cathode, CC: Current Con-
         troller, P: Micropump, PS: Power Supply, R: Rotame-
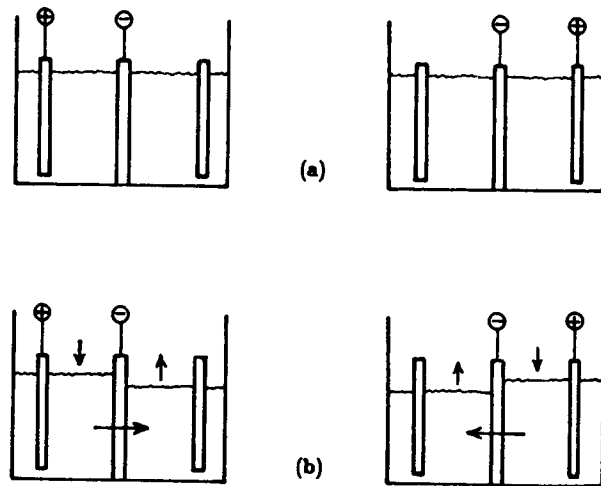   ter, RE: Reservoir).
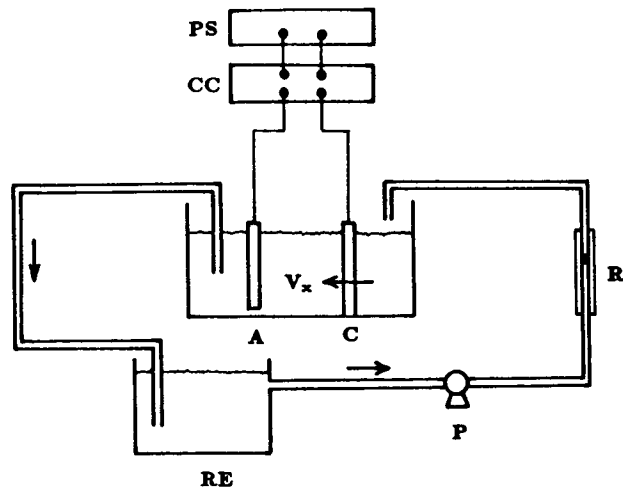
Figure 2. The Flow Rectangular–Type Cell with Anode Placed
         in Downstream (A: Anode, C: Cathode, CC: Current
         Controller, P: Micropump, PS: Power Supply, R: Ro-
         tameter, RE: Reservoir).

Figure 3. Electrode and Flow Configurations with Two–side
Impregnation for (a) Stagnant, and (b) Flow–Through
Upstream Counter.
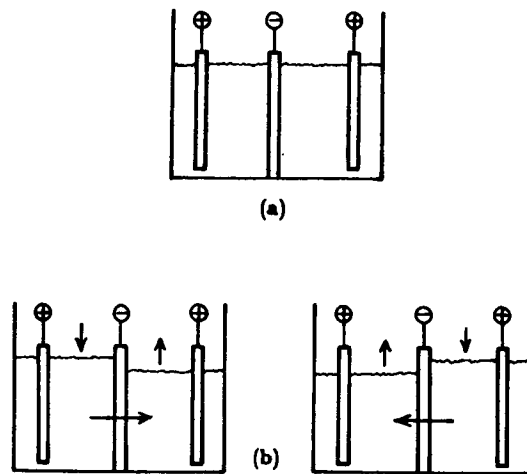
Figure 4. Electrode and Flow Configurations with Simultane-
ous Two–side Impregnation (a) Stagnant, and (b)
Flow–Through under Alternating Upstream–Downstream
Counterelectrode.
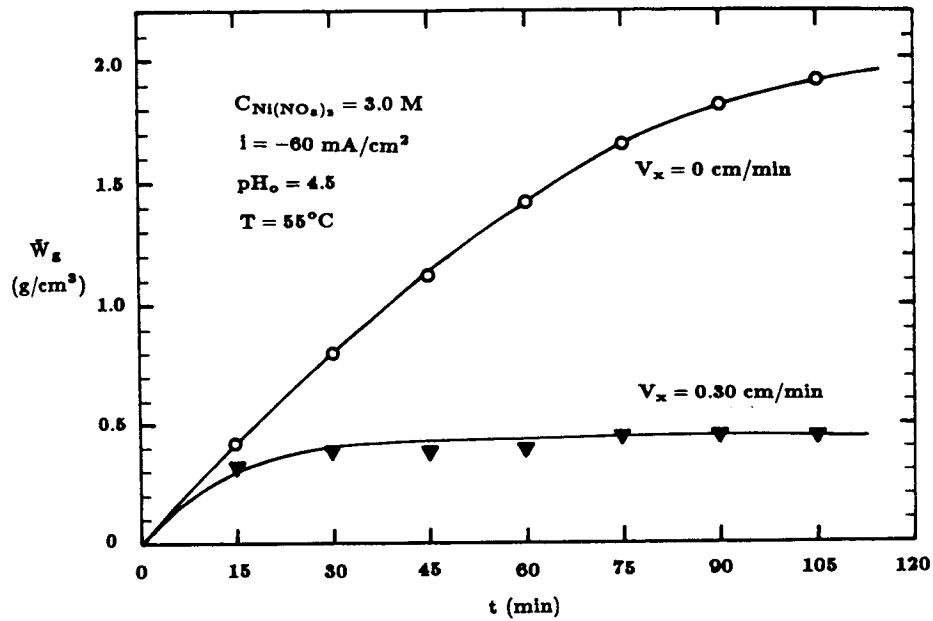
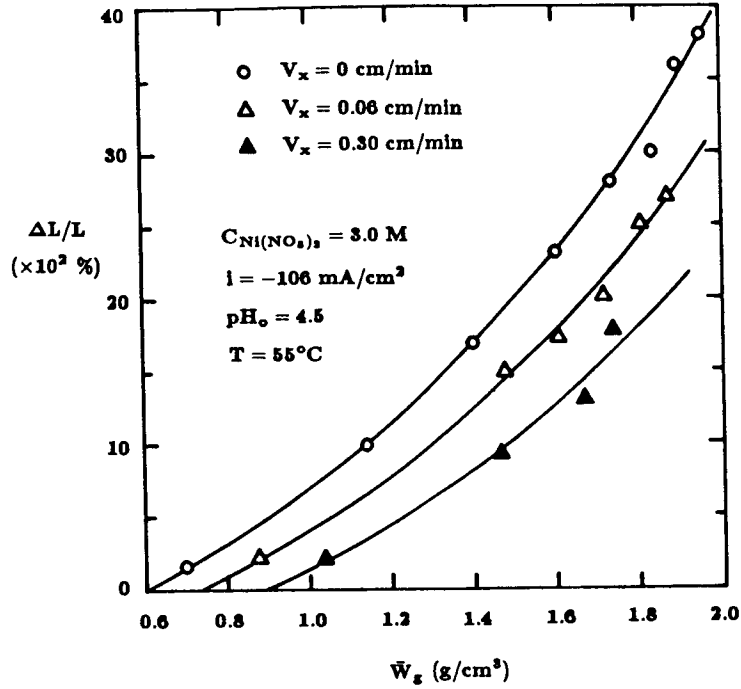Figure 5. Loading Level vs. Impregnation Time for Stagnant and Flow–Through Conditions in a Tube–Type Cell (Downstream Counter, $V_s/V_p = 2 \times 10^2$).
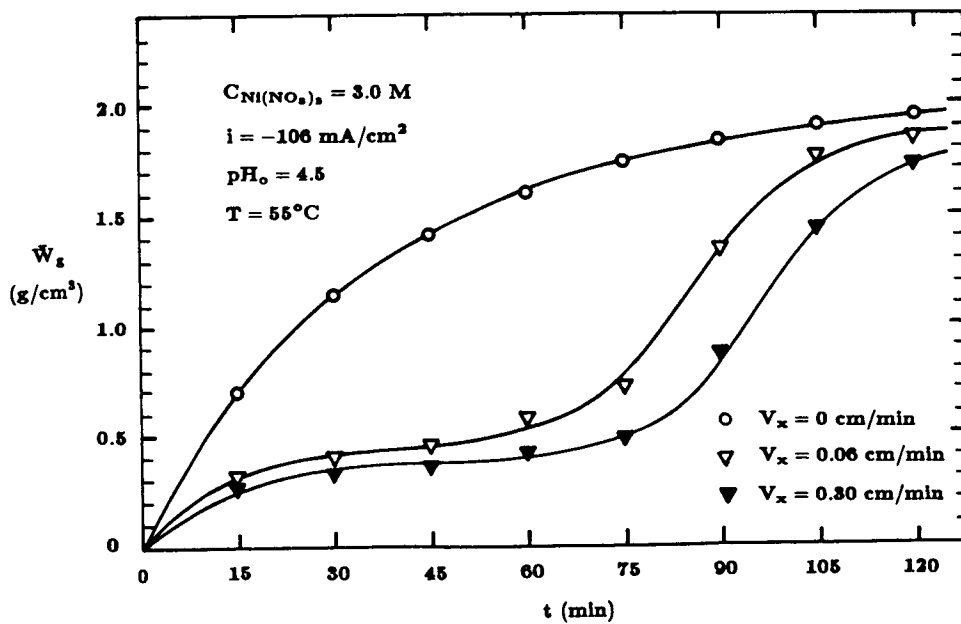
Figure 6. Loading Level vs. Impregnation Time for Stagnant and Flow–Through Conditions in a Rectangular–Type Cell at $pH_o = 4.5$ (Downstream Counter).
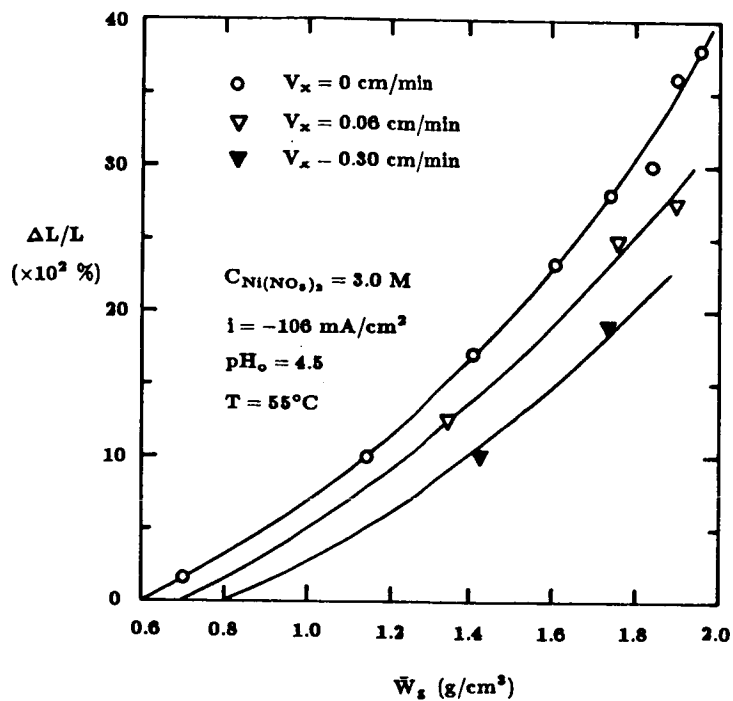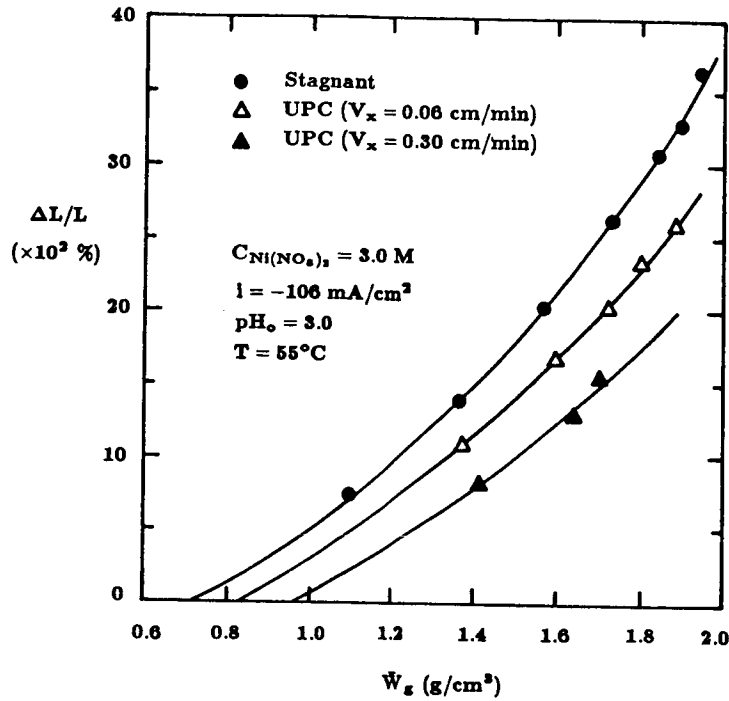
Figure 7. Plaque Expansion vs. Loading Level for Stagnant and Flow Conditions in a Rectangular–Type Cell at $pH_o = 4.5$ (Downstream Counter).
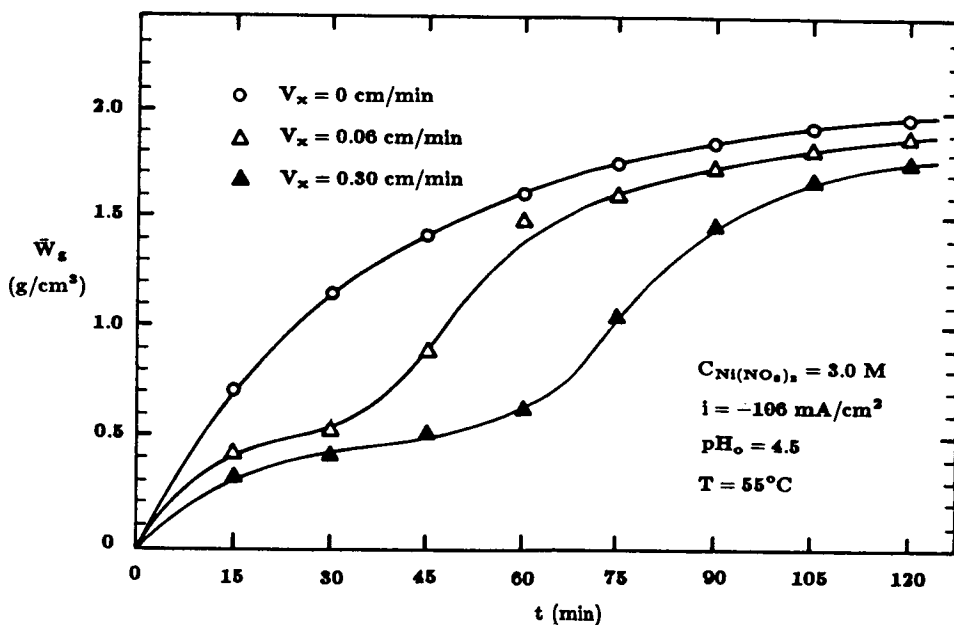
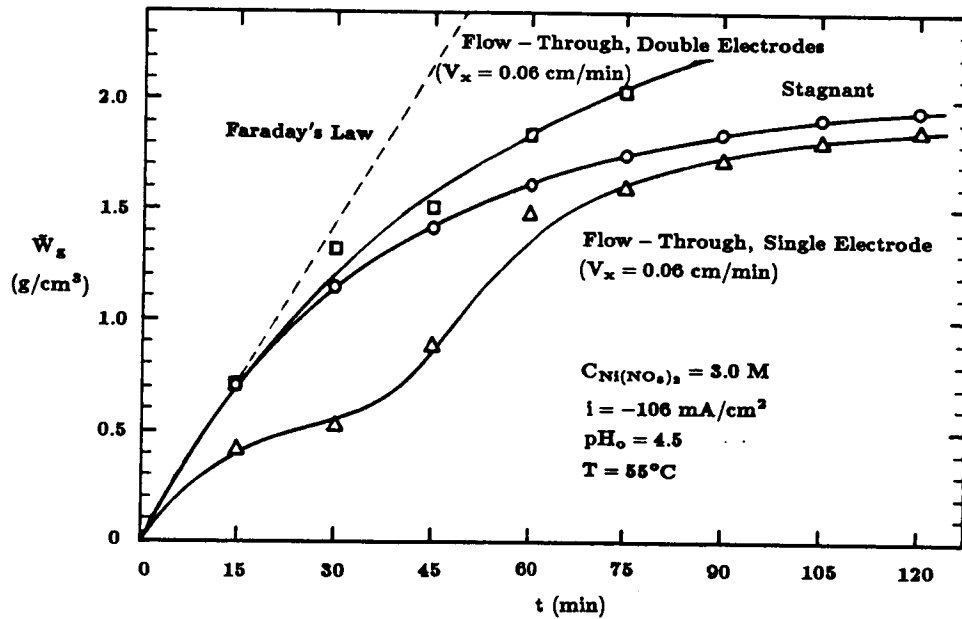Figure 8. Loading Level vs. Impregnation Time for Stagnant and Flow–Through Conditions in a Rectangular–Type Cell at $pH_o = 4.5$ (Upstream Counter).

Figure 9. Plaque Expansion vs. Loading Level for Stagnant and
Flow–Through Conditions in a Rectangular–Type Cell
at $pH_o = 4.5$ (Upstream Counter).
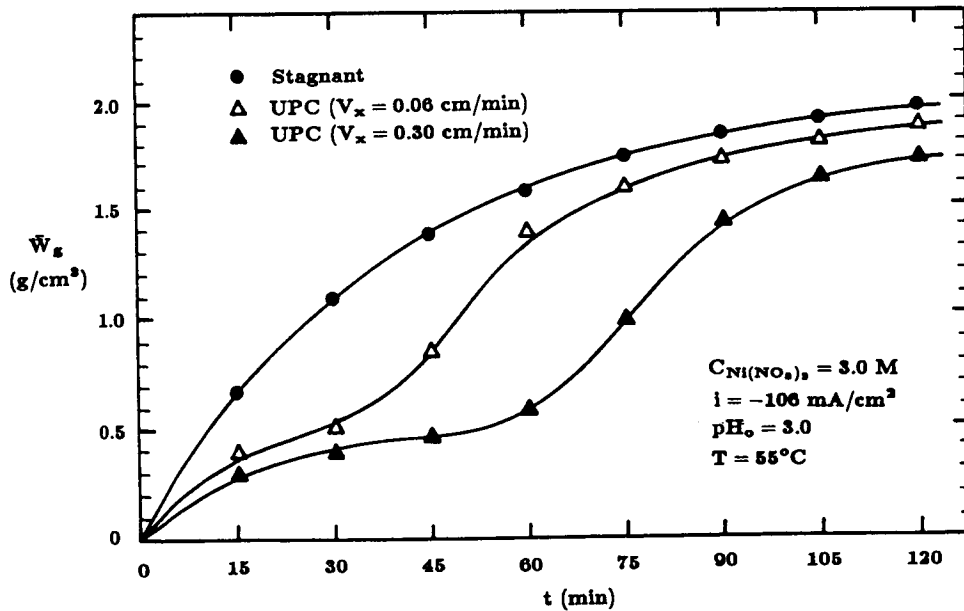
Figure 10. Loading Level vs. Impregnation Time for Stagnant and Flow–Through
Conditions in a Rectangular–Type Cell at $pH_o = 3.0$ (Upstream Counter).

Figure 11. Plaque Expansion vs. Loading Level for Stagnant and
Flow–Through Conditions in a Rectangular–Type Cell
at $pH_o = 3.0$ (Upstream Counter).

Figure 12. Loading Level vs. Impregnation Time for Stagnant, Flow–Through
Single Electrode, and Flow–Through Double Electrodes in a Rectangular–
Type Cell at $pH_o = 4.5$ (Upstream Counter).
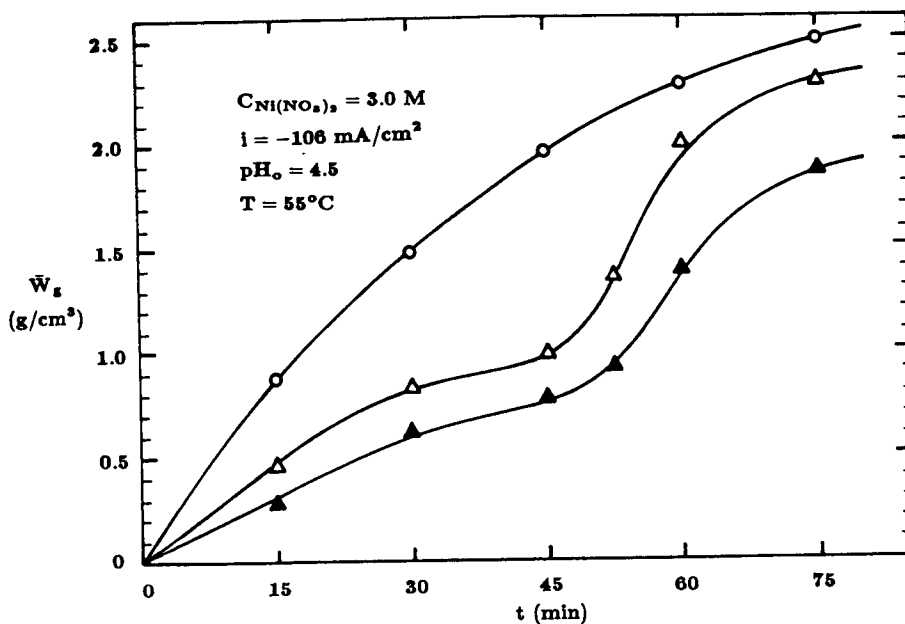
Figure 13. Loading Level vs. Impregnation Time for Stagnant and Flow-Through
Conditions (Upstream Counter) with Two-side Impregnation in a
Rectangular-Type Cell at $pH_o = 4.5$.

O Stagnant: each side impregnated with equal time.

△ Flow-Through: $V_x = 0.06$ cm/min, each side impregnated with equal time.

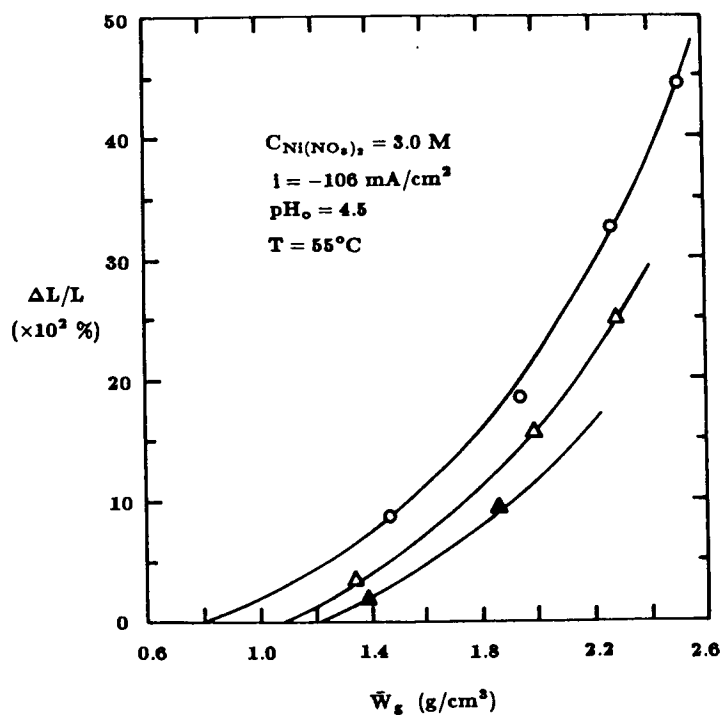▲ Flow-Through: $V_x = 0.06$ cm/min, each side impregnated periodically for 2.5 min .

Figure 14. Plaque Expansion vs. Loading Level for Stagnant and
Flow-Through Conditions (Upstream Counter) with
Two-side Impregnation in a Rectangular-Type Cell
at $pH_o = 4.5$ (Captions Are the Same as in Figure 5-
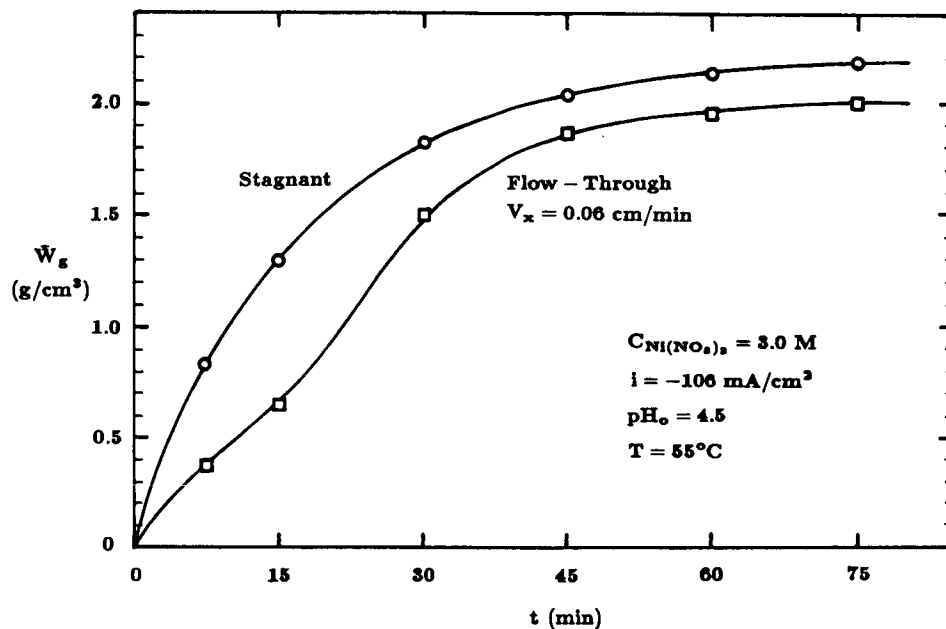13).

302

Figure 15. Loading Level vs. Impregnation Time for Stagnant and Flow-Through Conditions with Simultaneous Two-side Impregnation in a Rectangular-Type Cell at $pH_o = 4.5$.
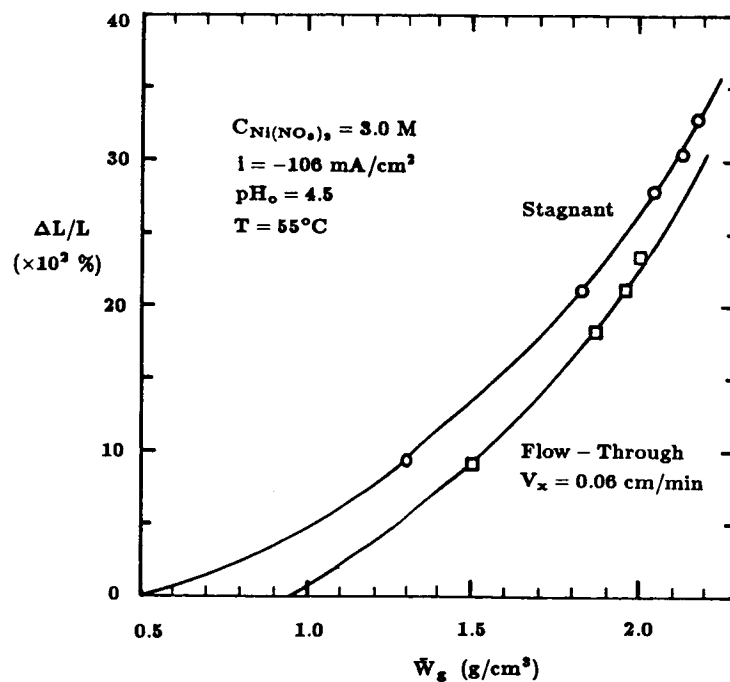

Figure 16. Plaque Expansion vs. Loading Level for Stagnant and Flow-Through Conditions with Simultaneous Two-side Impregnation in a Rectangular-Type Cell at $pH_o = 4.5$.
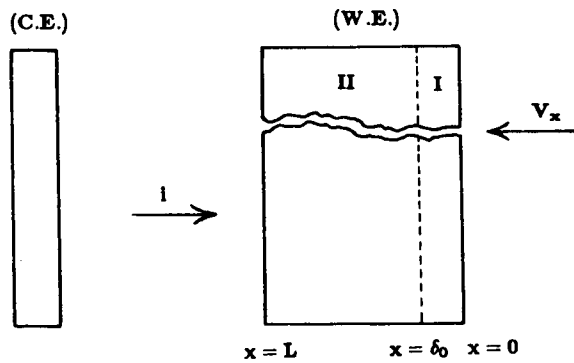
Figure 17. Schematic Representation of Electrochemical Precipitation within a Flow–Through Porous Electrode.